

# Memory in a sequence of weak and short duration measurements of non-commuting observables

Sophia M. Walls and Ian J. Ford

*Department of Physics and Astronomy, University College London,  
Gower Street, London, WC1E 6BT, United Kingdom*

Sequential projective measurements of non-commuting observables destroy information about previous measurement outcomes, but weak measurements conducted over short durations do not cause as much disturbance to the system, and as a result, memory of previous outcomes may not be entirely eliminated. We use Quantum State Diffusion to unravel a Lindblad equation, generating numerical, stochastic trajectories for two separate systems: a spin 1/2 system and a system of two entangled spin 1/2 subsystems, each undergoing a sequence of measurements of  $S_z$  and  $S_x$  spin observables  $S_z, S_x, S_z, S_x, \dots$ . The autocorrelation function of completed  $S_z$  measurement outcomes for a range of lag times is then calculated. In a second set of trajectories, the simulation is terminated if the system reaches the vicinity of a chosen set of eigenstates of  $S_z$  and  $S_x$ : the ‘terminating eigenstates’, during the respective measurement intervals of the two observables. Two quantities are then calculated from the generated trajectories, the ‘probability of termination’ that the system will arrive at one of the terminating eigenstates after a certain number of measurements have been performed, and the mean first passage, which is the number of measurements performed, on average, before the simulation ends. Results can then be compared with projective measurement Born rule statistics. We demonstrate that with short and weak measurements the autocorrelation function of  $S_z$  can be non-zero for a range of lag times, while it vanishes for strong, longer duration measurements in agreement with the Born rule. The probability of termination and the mean first passage increase under weaker and shorter measurements, revealing that the system is able to avoid particular eigenstates of  $S_z$  and  $S_x$  for extended periods of time. A bias can develop in favour of a return to the same eigenstate visited in the previous measurement(s) of a given observable: a memory effect.

## I. INTRODUCTION

Non-commuting observables are considered to be a hallmark of quantum mechanics. Unlike classical, Newtonian mechanics, conjugate variables such as position and momentum cannot simultaneously be measured precisely, due to the constraints of the Heisenberg uncertainty principle [1, 2]. Furthermore, a sequence of strong, projective measurements of non-commuting observables destroys information about previous measurement outcomes of the respective observables. Figure 1 demonstrates how the first  $\sigma_z$  measurement outcome at Stern-Gerlach device 1 (STG1) acting on a beam of spin 1/2 particles is destroyed, or ‘forgotten’, due to the non-commuting  $\sigma_x$  measurement at STG2. Only the  $\sigma_z$  Down  $|-\rangle_z$  outcomes at STG1 are passed through to STG2, yet the second  $\sigma_z$  measurement at STG3 has an equal split between Up  $|+\rangle_z$  and Down  $|-\rangle_z$  outcomes. Memory of the  $\sigma_z$  Down outcome at STG1 is completely erased by the  $\sigma_x$  measurement at STG2. Naturally this is reflected in the mathematics by the fact that  $\sigma_x$  Up eigenstates can be written as an equal superposition of  $\sigma_z$  eigenstates:  $|+\rangle_x = \frac{1}{\sqrt{2}}(|+\rangle_z + |-\rangle_z)$ .

The simultaneous and sequential measurement of non-commuting observables has recently been explored owing to its utility in understanding realistic quantum systems interacting with their environment through channels specified by non-commuting operators, as well as for applications in quantum cryptography [3–15]. Such investigations not only aid a deeper understanding of quan-

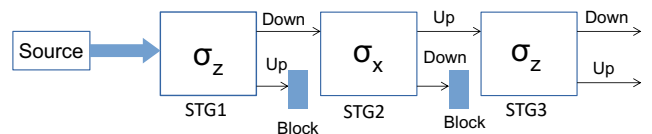


Figure 1. A demonstration of memory erasure in a sequence of strong, projective measurements of non-commuting observables  $\sigma_z$  and  $\sigma_x$  that remove information about previous measurement outcomes. Stern-Gerlach devices 1 (STG1) and 3 (STG3) conduct  $\sigma_z$  measurements whilst STG2 performs a  $\sigma_x$  measurement. The block prevents  $\sigma_z$  Up  $|+\rangle_z$  states from proceeding into STG2 such that only Down  $|-\rangle_z$  states can pass through. The second block prevents  $\sigma_x$  Down  $|-\rangle_x$  states from passing through to STG3. Memory erasure is seen in the  $\sigma_z$  measurement outcomes: despite only  $\sigma_z$  Down  $|-\rangle_z$  states being permitted access to STG2, after a second  $\sigma_z$  measurement at STG3, both Up and Down measurement outcomes emerge. The source of this randomness and ‘forgetting’ is the projective  $\sigma_x$  measurement at STG2 in between the two  $\sigma_z$  measurements.

tum foundations such as the measurement problem and the Heisenberg uncertainty principle, but it also proves to have a useful application in direct measurement of the elements of a density matrix of a quantum system and quantum state tomography [7, 16–20], as well as quantum error correction and quantum cybersecurity [21–24]. Calderón-Losada *et al* were able to assign simultaneously measured values of two non-commuting observables to particles in an EPR setting using weak measurements,

whilst Howell *et al* demonstrated that the EPR setting violates Heisenberg’s uncertainty principle [25, 26]. Similarly, measurements of non-commuting observables on a single particle have been performed using weak measurements to establish ‘weak value’ correlators across measurement outcomes or to demonstrate a violation of Heisenberg’s uncertainty principle [4, 8, 27, 28]. In addition, these measurement protocols have been used to demonstrate violations of the Leggett-Garg inequality [29, 30] and to test quantum contextuality [31–33]. Hossenfelder *et al* also proposed a scheme involving a sequence of measurements of non-commuting observables, to test whether non-zero correlations could exist in the autocorrelation function of measurement outcomes of the same observable at different times [34].

Whilst conventional quantum mechanics focuses on strong, projective, instantaneous measurements, and averages which mask what happens during single measurements, continuous quantum trajectories under weak measurement offer a framework in which quantum measurement takes place within a finite time and a system single evolution pathway may be tracked [35–37]. As such, the measurement strength and measurement period can be varied and possible memory effects may be explored that would otherwise be hidden by considering average system evolution. For example, if the measurement is too short or too weak, it may not disturb the system as much as a strong, projective measurement, and may be incomplete. Correlations between previous measurement outcomes of the same observable in a sequence of measurements of non-commuting observables may therefore not be destroyed. Incomplete measurements have been studied before using quantum trajectories in relation to the partial quantum Zeno effect, for example [38, 39], as well as to investigate the reversal of quantum measurements whereby the system returns to the state it was in previously after a partial collapse [37, 40–42]. In this work we utilise stochastic quantum trajectories to investigate whether memory of previous measurement outcomes of an observable can be retained in a sequence of weaker and shorter measurements of non-commuting observables.

Many techniques exist for generating quantum trajectories, such as the Feynman-Vernon path integral formalism, hierarchical equations of motion, and various unravellings of the Lindblad master equation such as the discontinuous jump trajectories and jump-time unravellings. The Liouville-von Neumann equation is a further example, though it does not preserve positivity and thus the trajectories generated cannot be considered as physically realistic [43–48]. In this work we generate stochastic, continuous and diffusive quantum trajectories using Quantum State Diffusion (QSD) which is a continuous unravelling of the Lindblad master equation [49].

In QSD, measurement arises when an open quantum system is coupled to an environment under dynamics designed to make it a measurement apparatus. The system-environment coupling therefore acts as a measurement strength that can be varied [50] in magnitude as a func-

tion of time [51]. The interaction with the environment drives the system towards particular eigenstates of the observable in a continuous and diffusive manner such that the completion of measurement takes a finite amount of time. The system’s evolution is described by a stochastic differential equation (SDE) that includes terms denoting interactions with the environment and therefore the effect of measurement on the system. In the absence of interactions with the environment system evolution is described by the von Neumann equation. The SDE generates single stochastic trajectories such that the average over all trajectories generated by the environmental noise yields the Lindblad master equation [50]. There has been a long-standing debate regarding the ontological status of the wavefunction and therefore whether quantum trajectories can be considered to be physically meaningful; in this work we interpret the wavefunction to be a physical property of the system and therefore regard quantum trajectories as real [36, 37, 52–59].

We utilise QSD to generate stochastic quantum trajectories for two separate systems: a spin 1/2 system and a system of two entangled spin 1/2 subsystems, both undergoing sequential measurements of  $S_z$  and  $S_x$  observables, namely  $S_z, S_x, S_z, S_x...$  with varying measurement strength and measurement period. The autocorrelation function of measurement outcomes of  $S_z$  can then be calculated, as well as the varying entanglement between the two-spin 1/2 subsystems. A second set of trajectories can then be generated where the simulation is ended if the system reaches the vicinity (within  $\pm 0.1$  of the eigenvalue) of certain eigenstates of the  $S_z$  or  $S_x$  observables - the ‘terminating’ eigenstates - during their respective measurement intervals, representing the ‘block’ in Figure 1. To demonstrate memory of previous measurement outcomes of the same observable, a number of quantities illustrating correlations between outcomes can then be found. In particular, we focus on the probability of termination defined as the probability that the simulation will run for a given time until the system moves into the vicinity of one of the terminating eigenstates. We also compute the mean first passage, which is the mean number of measurements performed before the simulation ends.

The plan for the paper is as follows: section II outlines the QSD framework and general SDE used to generate quantum trajectories; section III introduces the SDEs specific to the spin 1/2 system and the system of two entangled spin 1/2 subsystems; section IV describes the protocol for generating sequential measurements of non-commuting observables and finally sections V and VI present our results and conclusions.

## II. QUANTUM STATE DIFFUSION AND STOCHASTIC LINDBLAD EQUATIONS

Open quantum systems adopt uncertain states due to their interactions with an underspecified environment. In

such circumstances they can be modelled using a randomly evolving density matrix, whose (Markovian) evolution in a time increment  $dt$  is described by the super-operator  $\hat{S}[\rho]$ , involving Kraus operators  $M_j$  representing the possible system transitions resulting from the system dynamics and system-environment interactions [2, 60]:

$$\begin{aligned}\hat{S}[\rho(t)] &= \rho(t+dt) = \sum_j M_j(dt)\rho(t)M_j^\dagger(dt) \\ &= \sum_j p_j \frac{M_j(dt)\rho(t)M_j^\dagger(dt)}{\text{Tr}(M_j(dt)\rho(t)M_j^\dagger(dt))}.\end{aligned}\quad (1)$$

Such an evolution is positive and trace-perserving when the Kraus operators satisfy the completeness condition  $\sum_j M_j^\dagger(dt)M_j(dt) = \mathbb{I}$ . Eq. 1 can be interpreted in a framework where transitions from  $\rho(t)$  to one of several possible states  $M_j\rho(t)M_j^\dagger/\text{Tr}(M_j\rho(t)M_j^\dagger)$  at time  $t+dt$ , occur with probability  $p_j = \text{Tr}(M_j\rho(t)M_j^\dagger)$  [51]. To generate diffusive, continuous trajectories we consider Kraus operators of the form  $M_j \equiv M_{k\pm} = \frac{1}{\sqrt{2}}(\mathbb{I} \pm A_{k\pm})$ ,  $A_{k\pm} = -iH_s dt - \frac{1}{2}L_k^\dagger L_k dt \pm L_k \sqrt{dt}$ , the index  $k$  representing Lindblad channels, each of which is associated with two Kraus operators labelled by  $\pm$  [51, 61–64]. The system Hamiltonian is denoted by  $H_s$  and the Lindblad operators as  $L_k$ . Utilising such Kraus operators in the map in Eq. 1 and averaging over multiple trajectories leads to the usual Lindblad equation representing the average system evolution.

Due to the underspecified environment, the initial and final states of the system associated with the timestep  $dt$  are uncertain, and we need to consider an ensemble of possible states the system can adopt at each point in time, with the average density matrix over the ensemble then denoted as  $\bar{\rho}(t)$ . The action of a single Kraus operator  $M_j$  on a single member of the ensemble  $\rho(t)$  represents the transition

$$\rho(t+dt) = \rho(t) + d\rho = \frac{M_j(dt)\rho(t)M_j^\dagger(dt)}{\text{Tr}(M_j(dt)\rho(t)M_j^\dagger(dt))}, \quad (2)$$

and a sequence of single Kraus operators acting on a single member of the ensemble  $\rho$  then yields a stochastic trajectory. Note that the above map used with Kraus operators of the form  $M_j$  has been demonstrated to preserve positivity [51]. The average over all possible system transitions and ensemble of states  $\bar{\rho}(t+dt) = \sum_j M_j \bar{\rho}(t) M_j^\dagger$ , would then yield the Lindblad master equation [62]

$$d\bar{\rho} = -i[H_s, \bar{\rho}]dt + \sum_k \left( (L_k \bar{\rho} L_k^\dagger - \frac{1}{2}\{L_k^\dagger L_k, \bar{\rho}\}) dt. \right) \quad (3)$$

Using the map in Eq. 2 with Kraus operators  $M_j$ , such a Lindblad equation may be unravelled to obtain the following stochastic differential equation for quantum state diffusion:

$$\begin{aligned}d\rho &= -i[H_s, \rho]dt + \sum_k \left( (L_k \rho L_k^\dagger - \frac{1}{2}\{L_k^\dagger L_k, \rho\}) dt \right. \\ &\quad \left. + (\rho L_k^\dagger + L_k \rho - \text{Tr}[\rho(L_k + L_k^\dagger)]\rho) dW_k \right). \quad (4)\end{aligned}$$

The evolution of  $\rho$  is thus described by an Itô process with Wiener increments  $dW_k$  (one for each Lindblad operator or channel  $k$ ) [49, 50]. The Lindblad operators arise from system-environment interactions and thus stochasticity enters due to the effect of an uncertain environment on the system. The von Neumann equation for closed quantum system evolution is recovered when there are no system-environment interactions. A single trajectory is associated with a particular realisation of the noise and the Lindblad equation is recovered as an average over the noise.

### III. SYSTEM SPECIFICATION

For simplicity we consider a system with  $H_s = 0$  and two Lindblad operators  $L_x = aS_x$  and  $L_z = bS_z$  where the  $S_i$  are spin component operators and  $a$  and  $b$  are scalar coefficients representing the system-environment coupling and hence the strength of  $S_x$  and  $S_z$  measurements, respectively. Each Lindblad is associated with Wiener increments  $dW_x$  and  $dW_z$ , respectively, in the dynamics. When inserted into Eq. 4, we obtain the following SDE [63]

$$\begin{aligned}d\rho &= a^2 \left( S_z \rho S_z - \frac{1}{2} \rho S_z^2 - \frac{1}{2} S_z^2 \rho \right) dt + \\ &\quad + b^2 \left( S_x \rho S_x - \frac{1}{2} \rho S_x^2 - \frac{1}{2} S_x^2 \rho \right) dt + \\ &\quad + a (\rho S_z + S_z \rho - 2\langle S_z \rangle \rho) dW_z + \\ &\quad + b (\rho S_x + S_x \rho - 2\langle S_x \rangle \rho) dW_x,\end{aligned}\quad (5)$$

where  $\langle S_i \rangle = \text{Tr}(\rho S_i)$ . Note that we do not consider  $\langle X \rangle$  to be an ‘expectation value’ in the conventional sense: namely as a statistical property of the dynamics. Rather we regard it as a physical attribute of the current quantum state  $\rho$  of the system [51]; a stochastically evolving property of the system.

#### A. Spin 1/2 system

The density matrix of a spin 1/2 system can be built using the Bloch sphere formalism of Aerts and de Bianchi, writing  $\rho = \frac{1}{2}(\mathbb{I} + \mathbf{r} \cdot \boldsymbol{\sigma})$ , where  $\mathbf{r} = (r_x, r_y, r_z)$  is the coherence vector  $\mathbf{r} = \text{Tr}(\rho \boldsymbol{\sigma})$  and  $\boldsymbol{\sigma} = (\sigma_x, \sigma_y, \sigma_z)$  is a vector of Pauli matrices [65]. Using  $d\mathbf{r} = \text{Tr}(d\rho \boldsymbol{\sigma})$ , and Eq. 5, we can derive SDEs for the coherence vector components. We choose  $r_y = 0$ ,  $dr_y = 0$  for simplicity and obtain the following SDEs [20],

## B. System of two entangled spin 1/2 subsystems

In order to construct the density matrix of the entangled two-spin 1/2 subsystems, we utilise SU(4) generators in the generalised Bloch sphere representation [65]:

$$\begin{aligned} dr_z &= 2a(1 - r_z^2)dW_z - 2b^2r_zdt - 2br_zr_xdW_x \\ dr_x &= 2b(1 - r_x^2)dW_x - 2a^2r_xdt - 2ar_xr_zdW_z. \end{aligned} \quad (6)$$

$$\rho = \frac{1}{4}(\mathbb{I} + \mathbf{s} \cdot \mathbf{\Sigma}). \quad (7)$$

The 15 component coherence vector is  $\mathbf{s} = (v, e, f, g, h, j, k, l, m, n, o, p, q, s, u)$  and the vector of generators  $\mathbf{\Sigma}$  has components  $\Sigma_m$  with  $m = 1, 15$ , constructed using the tensor product of two Pauli matrices:  $\Sigma_m = \sigma_i \otimes \sigma_j$ : full details are given in Appendix A. The following density matrix is then obtained for the entangled two-spin 1/2 system:

Stochastic trajectories in the  $(r_x, r_z)$  phase space are then generated using these SDEs.

$$\rho = \frac{1}{4} \begin{pmatrix} 1 + f + p + u & -ie + q - is + v & g + k - il - io & h - ij - im - n \\ ie + q + is + v & 1 - f + p - u & h + ij - im + n & g - k - il + io \\ g + k + il + io & h - ij + im + n & 1 + f - p - u & -ie - q + is + v \\ h + ij + im - n & g - k + il - io & ie - q - is + v & 1 - f - p + u \end{pmatrix}. \quad (8)$$

As before, stochastic quantum trajectories can be produced from the equations of motion of the 15 variables parametrising the density matrix. SDEs for components of the coherence vector  $s_m$  are obtained through

$$ds_m = Tr(d\rho\Sigma_m). \quad (9)$$

The full set of SDEs can be found in Appendix B. A useful visualisation of the evolution is obtained by considering trajectories in the  $(\langle S_x \rangle, \langle S_z \rangle)$  coordinate space. Using  $\langle X \rangle = Tr(X\rho)$ , and  $S_z = \sigma_{z,1} \otimes \mathbb{I} + \mathbb{I} \otimes \sigma_{z,2}$  where subscripts 1 and 2 label the first and second spin 1/2 subsystem, we obtain

$$\langle S_z \rangle = \frac{f + p}{2} \quad (10)$$

$$\langle S_x \rangle = \frac{g + v}{2} \quad (11)$$

$$\langle S_y \rangle = \frac{e + l}{2} \quad (12)$$

$$\langle S^2 \rangle = \frac{1}{2}(3 + h + n + u). \quad (13)$$

The entanglement can be revealed by considering the von Neumann entropy  $S_{vN}$  of the reduced density matrices of the individual spin 1/2 subsystems,  $\rho_{A,B}$ , such that  $S_{vN}(\rho_A) = S_{vN}(\rho_B) = -\sum_j \lambda_j \log(\lambda_j)$ , where the subscripts  $A$  and  $B$  denote the first and second spin 1/2 subsystems and  $\lambda_j$  denote the eigenvalues of their reduced density matrices. These can be written as

$$\begin{aligned} \rho_A &= \frac{1}{2} \begin{pmatrix} 1 + p & g - il \\ g + il & 1 - p \end{pmatrix} \\ \rho_B &= \frac{1}{2} \begin{pmatrix} 1 + f & v - ie \\ v + ie & 1 - f \end{pmatrix}, \end{aligned} \quad (14)$$

and the von Neumann entropy can be expressed as

$$\begin{aligned} S_{vN}(\rho_A) &= 1 + \frac{1}{\ln(4)}((-1 + \mu)\ln(1 - \mu) \\ &\quad - (1 + \mu)\ln(1 + \mu)) \\ \mu &= \sqrt{g^2 + l^2 + p^2} \\ S_{vN}(\rho_B) &= 1 + \frac{1}{\ln(4)}((-1 + \eta)\ln(1 - \eta) \\ &\quad - (1 + \eta)\ln(1 + \eta)) \\ \eta &= \sqrt{e^2 + f^2 + v^2}, \end{aligned} \quad (15)$$

where  $\mu$  and  $\eta$  are formed from the three variables parametrising the reduced density matrices  $\rho_A$  and  $\rho_B$ .

## IV. PROTOCOL TO GENERATE SEQUENTIAL MEASUREMENTS OF NON-COMMUTING OBSERVABLES

In order to generate a sequence of alternating measurements of the non-commuting observables  $S_z$  and  $S_x$ , we assign the measurement strengths  $a(t)$  and  $b(t)$  to be time-varying box functions, such that when  $a = 1$ ,  $b = 0$

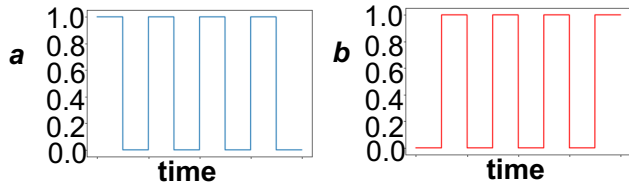


Figure 2. The evolution of measurement strengths  $a$  and  $b$  for the observables  $S_x$  and  $S_z$  respectively. In order to produce sequential measurements of the non-commuting observables, the measurement strengths are modelled as box functions such that when  $a = 1$ ,  $b = 0$  and vice-versa. The period of the box function is referred to as the measurement period.

and vice-versa (see Figure 2). The period of the box function is henceforth referred to as the measurement period.

Stochastic quantum trajectories for the spin 1/2 system are generated in the phase space of the components of the coherence vector  $(r_x, r_z)$  whilst for the system of two entangled spin 1/2 subsystems, they are generated in the phase space of the spin components  $(\langle S_x \rangle, \langle S_z \rangle)$ .

In a first set of trajectories, the autocorrelation function of measurement outcomes is computed. For the system of two entangled spin 1/2 subsystems, a measurement outcome is defined to occur when  $\langle S_z \rangle$  for the system, for example, approaches within  $\pm 0.1$  of the eigenvalue of an eigenstate of  $S_z$  in an interval when an  $S_z$  measurement is conducted. The autocorrelation function is then calculated using only these successful  $S_z$  measurement outcomes, as follows:

$$C_{S_z}(l) = \frac{\sum_{n=1}^{N-l} (R_n - \bar{R})(R_{n+l} - \bar{R})}{\sum_{n=1}^N (R_n - \bar{R})^2}. \quad (16)$$

Here  $l$  is the lag time in units of the number of  $S_z$  measurements conducted,  $n$  denotes the number of  $S_z$  measurements performed and  $N$  is the total number of realised  $S_z$  measurements.  $R_n$  then denotes the value of  $\langle S_z \rangle$  of the system after  $n$  measurements have been performed and  $\bar{R}$  is the mean value of  $\langle S_z \rangle$ . A similar autocorrelation function can be defined for measurements of  $\sigma_z$  in the single spin 1/2 system.

In a second set of trajectories, the simulation is terminated if  $\langle \sigma_x \rangle$  for the spin 1/2 system reaches within  $\pm 0.1$  of the  $-1$  eigenstate of  $\sigma_x$  or  $\langle \sigma_z \rangle$  approaches within  $\pm 0.1$  of the  $+1$  eigenstate of  $\sigma_z$ , again in the appropriate measurement intervals. We will refer to such eigenstates that lead to the end of the simulation as the ‘terminating eigenstates’. For the entangled two-spin 1/2 system, there are more eigenstates available to the observables, and we choose two separate sets of terminating eigenstates. In the first set, the simulation terminates if  $\langle S_x \rangle$  for the system reaches within  $\pm 0.1$  of the  $S = 1, m_x = -1$  eigenstate of  $S_x$ , or  $\langle S_z \rangle$  reaches within  $\pm 0.1$  of the  $S = 1, m_z = -1$  eigenstate of  $S_z$ , where  $S$  is the total spin  $S = S_A + S_B$ , where  $A$  and  $B$  label the

two subsystems and  $m_x$  and  $m_z$  are the components of the spin projected onto the  $x$  and  $z$  axes, respectively. In the second set, the simulation terminates if  $\langle S_x \rangle$  for the system reaches within  $\pm 0.1$  of the  $S = 1, m_x = 0$  eigenstate of  $S_x$  or  $\langle S_z \rangle$  lies within  $\pm 0.1$  of the  $S = 1, m_z = 0$  eigenstate of  $S_z$ . Note that the first set of terminating eigenstates comprises eigenstates of  $S_x$  and  $S_z$  that are separable, i.e. they are products of eigenstates of the two spins, whilst the second set includes those that are entangled. In this way, we are able to study any differences that may result from the level of entanglement in the eigenstates. From this set of trajectories the following quantities can be calculated.

- The probability of termination: the probability that the system will arrive within the designated vicinity of the terminating eigenstates of  $S_z$  and  $S_x$ , during the observables’ respective measurement intervals, up to a time  $t$ .
- The mean first passage: the mean number of measurements performed before the system arrives within the designated vicinity of the terminating eigenstates of  $S_z$  and  $S_x$ .

## V. RESULTS

### A. Spin 1/2 system

Numerical trajectories were generated for the spin 1/2 system in the  $(r_x, r_z)$  phase space using the Euler-Maruyama update method [66]. An example trajectory is shown in Figure 3. The system begins at the centre of the circle in the totally mixed state. As  $\sigma_z$  and  $\sigma_x$  measurements are performed, the system purifies and evolves towards the circumference of the circle, where it remains for the remainder of its evolution. The  $\sigma_z$  eigenstates lie at the poles and the  $\sigma_x$  eigenstates at the equator such that when a  $\sigma_z$  measurement is conducted, the system evolves to one of its eigenstates and similarly for a measurement of  $\sigma_x$ .

When the measurement period is short, the measurement process may not be complete: the system may not arrive at the eigenstate of the observable that is being measured. This is illustrated in Figures 4a and b. Figure 4a shows a  $\sigma_z$  measurement being conducted on the system between times 18 and 19, causing the system to travel towards the  $+1$  eigenstate. Figure 4b then illustrates a  $\sigma_x$  measurement being performed between times 19 and 20, leading the system to move away from  $r_x = 0$ . However, it does not succeed in arriving at an eigenstate of  $\sigma_x$ , according to the criteria employed. Within the time interval 20-21, a second  $\sigma_z$  measurement is performed and in Figure 4a it can be seen that the system moves back to the  $+1$  eigenstate it adopted when the first  $\sigma_z$  measurement was conducted during the time interval 18-19. A  $\sigma_x$  measurement is made once again between times 21 and 22 in Figure, causing the system to travel

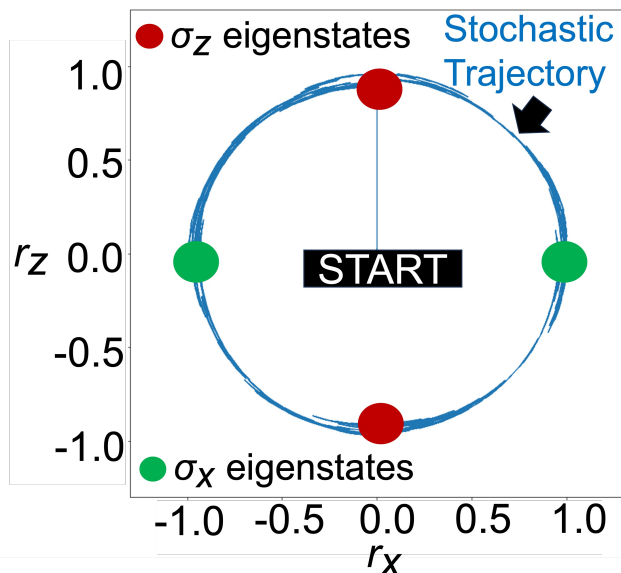


Figure 3. An example trajectory of the spin 1/2 system in the  $(r_x, r_z)$  phase space. The system starts in the mixed state at the centre of the Bloch sphere. When a measurement is performed, the system is purified and travels towards the circumference, where it remains. The  $\sigma_x$  eigenstates are at the equator whilst the  $\sigma_z$  eigenstates are at the poles.

towards a  $\sigma_x$  eigenstate but again it is not successful in doing so as can be seen in Figure 4b. As a result, when a third  $\sigma_z$  measurement is performed in interval 22-23, Figure 4a shows that the system once again arrives back at the +1 eigenstate of  $\sigma_z$ - the same eigenstate it was in at times 18-19 and 20-21 in the previous two measurements of  $\sigma_z$ . As a result of the  $\sigma_x$  measurements being unsuccessful in leading the system to a  $\sigma_x$  eigenstate, the system is allowed to return to the same eigenstate of  $\sigma_z$  multiple times. We can imagine such a scenario in the  $(r_x, r_z)$  phase space in Figure 3. After a  $\sigma_z$  measurement, the system is at the north pole where the +1 eigenstate of  $\sigma_z$  resides. When a  $\sigma_x$  measurement is then performed, but does not successfully bring the system to an eigenstate, the system then remains in the top half of the circle, meaning that when a second  $\sigma_z$  measurement is conducted shortly after, the system is more likely to return to the +1 eigenstate than the -1 eigenstate since it is closer to it. This is how memory might emerge.

Example trajectories expressed in the form of cumulative probability densities are illustrated in Figure 5. As the measurement strength and period are increased, the system spends more time in the vicinity of the eigenstates of  $\sigma_z$  and  $\sigma_x$  and the time spent in each of their respective eigenstates is equal (Figures 5, f, h, i). As the measurement period is shortened and the measurement strength is weakened, the system explores the edge of the circle more uniformly (Figure 5b) or shows a bias towards cer-

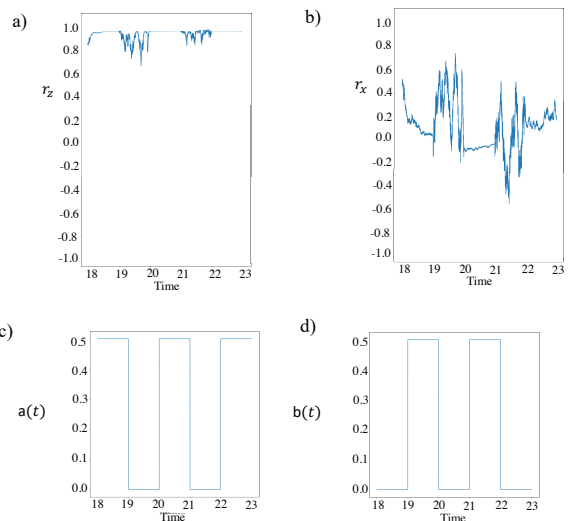


Figure 4. An example trajectory illustrating how the coherence vector components  $r_z$  and  $r_x$  vary with time, a) and b), alongside the evolution of c) the measurement strength  $a(t)$  and d) the measurement strength  $b(t)$ . Measurement period 2, duration 200, time-step 0.0001 were used. A measurement of  $\sigma_z$  starts at times 18, 20 and 22, whilst a measurement of  $\sigma_x$  starts at 19, 21 and 23.

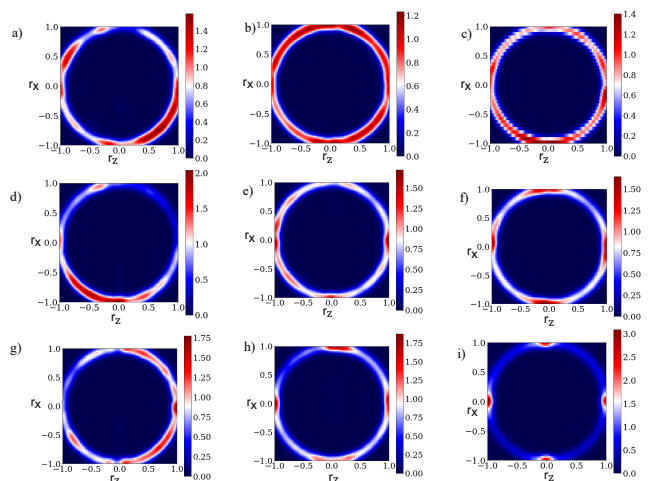


Figure 5. Color. Cumulative probability densities in the  $(r_x, r_z)$  phase space, arising from continuous stochastic trajectories for the spin 1/2 system under sequential measurement. Rows: measurement strength 0.5, 0.75 and 1 from left to right. Columns: measurement period 0.5, 1 and 2 from top to bottom. Duration 200, time-step 0.0001.

tain eigenstates of the observables than others (Figures 5a, d, e, g).

Figure 6 illustrates the autocorrelation function  $C_{\sigma_z}$  of  $\langle \sigma_z \rangle$  as a function of lag time in units of number of measurements performed. There is a significant correlation between the outcomes of  $\sigma_z$  for short measurement

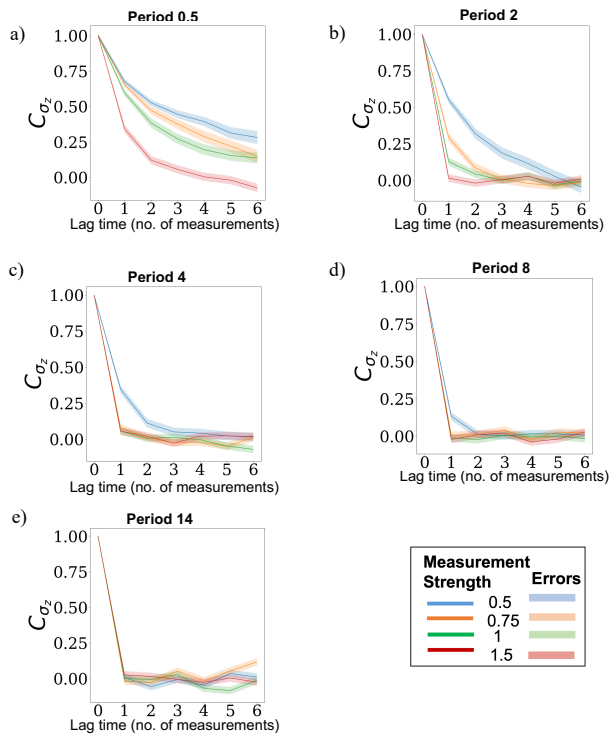


Figure 6. Color. The autocorrelation function  $C_{\sigma_z}$  of measurements of  $\sigma_z$  for the spin 1/2 system, as a function of number of measurements performed for varying measurement strengths and measurement periods. a) Measurement period 0.5: a short measurement period, correlations are exhibited, b) Measurement period 2, c) measurement period 4, d) measurement period 8, e) measurement period 10, f) Measurement period 14: there are no correlations and we recover Born rule statistics.

periods and weak measurements, demonstrating memory of previous  $\sigma_z$  outcomes despite the intervening  $\sigma_x$  measurements. Such correlations disappear when the measurement strength is increased or the measurement period is longer, such as in Figure 6e, since these situations more closely approximate to Born rule projective measurements. As the measurement strength is increased, the statistical error in the values of the autocorrelation function increases since the measurement term in Eq. 5, which includes a stochastic noise, increases as a result.

Now we introduce terminating eigenstates and generate a second set of trajectories by considering the simulation to end when  $\langle \sigma_x \rangle$  for the system reaches within  $\pm 0.1$  of the  $-1$  eigenvalue of  $\sigma_x$ , or  $\langle \sigma_z \rangle$  reaches the vicinity of the  $+1$  eigenstate of  $\sigma_z$ , during the appropriate measurement intervals. Figure 7 illustrates the probability that the system will reach one of these terminating eigenstates after a certain number of measurements have been performed (note that the first measurement corresponds to a  $\sigma_z$  measurement, the second to a  $\sigma_x$  measurement and the third to a  $\sigma_z$  measurement, etc). Figure 7i depicts

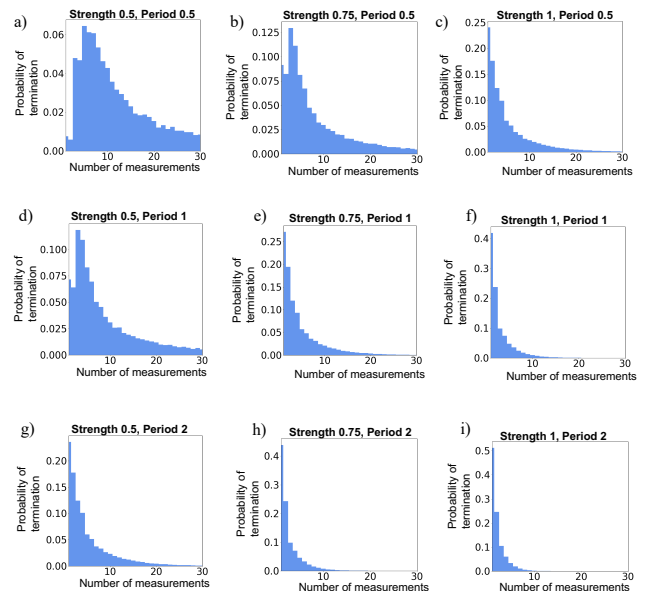


Figure 7. The probability of termination for the spin 1/2 system as a function of number of measurements performed. The probability of termination is defined as the probability that the  $\langle \sigma_x \rangle$  or  $\langle \sigma_z \rangle$  values of the system will reach within  $\pm 0.1$  of the  $-1$  eigenstate of  $\sigma_x$  or the  $+1$  eigenstate of  $\sigma_z$ , during the observables' respective measurement intervals and hence end the simulation. Note that the first measurement corresponds to a  $\sigma_z$  measurement, the second to a  $\sigma_x$  measurement and the third to a  $\sigma_z$  measurement, etc. It is illustrated for varying measurement strengths and measurement periods. Rows: measurement strength 0.5, 0.75 and 1 from left to right. Columns: measurement period 0.5, 1 and 2 from top to bottom. Generated using 24,000 trajectories, time-step 0.0001.

Born rule statistics since the measurement period is long and a strong measurement is being performed. However, as the measurement strength and period are decreased we see that there are deviations from Born rule statistics. Figure 7i shows a high probability for the system to arrive at a terminating eigenstate after only a small number of measurements have been performed and a probability close to zero after many rounds of measurements. In contrast, Figures 7a,b and 7d show that after a small number of measurements, the probability of reaching a terminating eigenstate is lower and the decrease in probability with number of measurements is not as steep. For example, after 30 measurements, Figure 7i suggests that the probability of reaching a terminating eigenstate is around  $\approx 9.3 \times 10^{-10}$ , compared with  $\approx 0.01$  in Figure 7a. Therefore, under non-projective measurement conditions, the system may be able to avoid particular eigenstates of the observables for a larger number of measurement intervals, potentially revealing a bias towards certain eigenstates than others.

From the trajectories generated in Figure 7, the mean

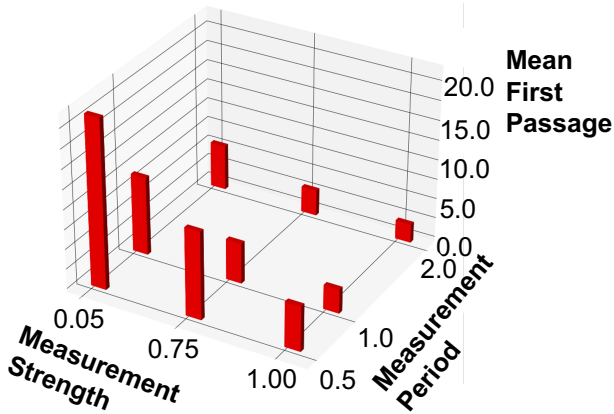


Figure 8. The mean first passage (mfp) for the spin 1/2 system is depicted for varying measurement strength and measurement period. It is defined as the average number of measurements performed before the simulation terminates due to the system arriving at either of the terminating eigenstates. The mfp is calculated from the trajectories in Figure 7.

first passage (mfp) is found as a function of measurement period and strength. This is defined as the mean number of measurements performed before the system reaches one of the terminating eigenstates and the simulation ends. From Figure 8, it can be seen that as the measurement strength and period decrease, the mfp increases: the system may be able to avoid certain eigenstates of the observables for longer with weaker, shorter measurements, reinforcing what was shown in Figure 7.

## B. System of two entangled spin 1/2 subsystems

Numerical trajectories for the entangled two-spin 1/2 system were generated in the  $(\langle S_x \rangle, \langle S_z \rangle)$  phase space. Figure 9 illustrates an example trajectory with the constraint  $S = 1, \langle S^2 \rangle = 2$ , where, as before,  $S = S_A + S_B$  and  $A$  and  $B$  label the first and second spin 1/2 subsystem, respectively. Only the triplet eigenstates of the  $S_x$  and  $S_z$  observables are available to the system. This is achieved by initialising the system in the mixed state  $\rho_{\text{start}} = \frac{1}{3}(|1\rangle_z \langle 1|_z + |-1\rangle_z \langle -1|_z + \frac{1}{2}(|1\rangle_z \langle -1|_z + |-1\rangle_z \langle 1|_z))$  such that there is a zero probability of reaching the  $S = 0$  singlet state, since  $\langle \Psi_{S=0} | \rho_{\text{start}} | \Psi_{S=0} \rangle = 0$ , and equal probabilities of reaching any of the three triplet eigenstates. Note that the dynamics are such that once the system reaches  $\langle S^2 \rangle = 2$  from its initial mixed state  $\rho_{\text{start}}$ , it remains at  $\langle S^2 \rangle = 2$  for the remainder of the simulation. The pattern of the trajectory is influenced by the many different possible eigenstates of  $S_x$  and  $S_z$  to which the system can evolve. For example, the red circles in Figure 9c depict how the system moves between different eigenstates of  $S_z$ , whilst the red circles in Figure 9e illustrate how the system travels between different eigenstates of  $S_x$ . Additionally, the red lines from the

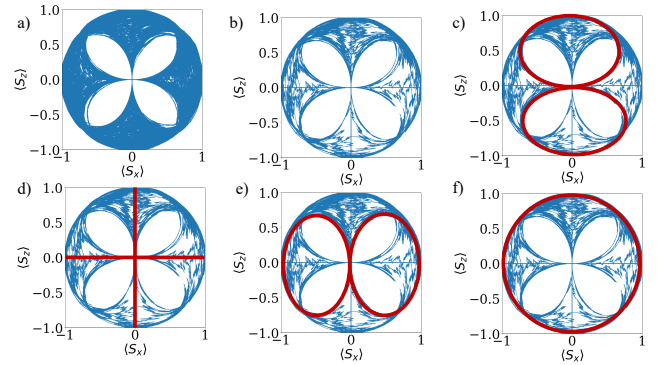


Figure 9. Color. a) Example trajectory of the system of entangled two spin 1/2 subsystems in the  $(\langle S_x \rangle, \langle S_z \rangle)$  phase space. Measurement strength 4, measurement period 2, duration 500, time-step 0.0001. Starting at  $\rho_{\text{start}} = \frac{1}{3}(|1\rangle_z \langle 1|_z + |-1\rangle_z \langle -1|_z + \frac{1}{2}(|1\rangle_z \langle -1|_z + |-1\rangle_z \langle 1|_z))$ , the system can never reach the singlet state and travels instead between the different triplet eigenstates of  $S_x$  and  $S_z$ . The  $m_x = 0$  and  $m_z = 0$  eigenstates are at the centre of the circle, whilst the  $m_x = \pm 1$  eigenstates are at the equator and the  $m_z = \pm 1$  eigenstates are at the poles. b) Shorter example trajectory, measurement strength 4, measurement period 2, duration 80, time-step 0.0001. The principal patterns of evolution are illustrated in c)-f). c) The system moves between the eigenstates of  $S_z$  by means of the two red circles. d) The system moves by means of the red lines between the maximally entangled eigenstates of  $S_x$  of the two spin 1/2 subsystems that lie at the centre of the circle and the separable eigenstates of  $S_z$  that lie on its surface (and vice-versa). e) The red circles here represent how the system evolves between different eigenstates of  $S_x$ . f) The large red circle around the edge of the circle illustrates how the system evolves between all the separable eigenstates of  $S_x$  and  $S_z$ , all of which lie on its circumference.

centre to the edge of the circle in 9d illustrate system evolution between the maximally entangled eigenstates of  $S_x$  (or  $S_z$ ) of the two spin 1/2 subsystems at the centre of the circle, to the separable (product) eigenstates of  $S_z$  ( $S_x$ ) at the edge of the circle. Finally the red circle around the circumference in Figure 9f is formed as the system moves between all the separable eigenstates of  $S_z$  and  $S_x$ .

Similarly to the spin 1/2 system, we can explore the trajectories formed in the  $(\langle S_x \rangle, \langle S_z \rangle)$  phase space through a probability density. Figure 10 depicts how the trajectories and cumulative probability density vary with measurement strength and measurement period. For longer measurement period and measurement strength, shown in Figure 10i, there is a higher probability density around the eigenstates of  $S_x$  and  $S_z$  and the pattern seen in Figure 9a is recovered. In accordance with the Born rule, the probability around the centre is twice as large as around the other eigenstates, since both the  $S = 1, m_x = 0$  and the  $S = 1, m_z = 0$  eigenstates reside there. As the measurement period and the measurement strength are decreased, the probability density spreads

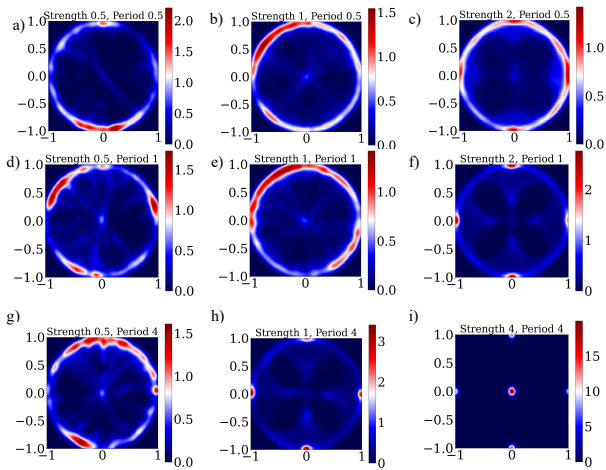


Figure 10. Color. Trajectories of the system of two entangled spin 1/2 subsystems in the  $(\langle S_x \rangle, \langle S_z \rangle)$  phase space represented in the form of a cumulative probability density. Duration 500, time-step 0.0001. Rows: measurement period 0.5, 1 and 4 from left to right. Columns: measurement strength 0.5, 1 and 2 from top to bottom.

into areas more distant from the eigenstates. The maximally entangled  $S = 1, m_x = 0$  and  $S = 1, m_z = 0$  eigenstates of the two spin 1/2 subsystems are, in particular, explored less frequently. Note that maximal entanglement means that the two spin 1/2 subsystems in the system are entangled with one another, not that the system is entangled with its environment, since the system eigenstates become pure. The probability density may also be concentrated around certain eigenstates of the observables and not others, potentially demonstrating a bias in return to those eigenstates in particular.

Another interesting property of the system of two entangled spin 1/2 subsystems that can be explored is the extent of entanglement between the two spins, as represented by the von Neumann entropy of the reduced density matrix of the first or second spin 1/2 subsystem. A trajectory in the  $(\langle S_x \rangle, \langle S_z \rangle)$  phase space with an indication of entanglement is illustrated in Figure 11. The entanglement is lowest on the circumference of the circle where the separable eigenstates of  $S_z$  and  $S_x$  lie, and highest at the centre, where the maximally entangled  $S = 1, m_x = 0$  and  $S = 1, m_z = 0$  eigenstates of the two spin 1/2 subsystems reside. There is a clear increase in the entanglement when the system evolves towards the centre of the circle.

Figure 12 illustrates the autocorrelation function  $C_{S_z}$  of  $\langle S_z \rangle$ , against the lag time in units of the number of measurements performed.  $C_{S_z}$  was calculated from the measurement outcomes of  $\langle S_z \rangle$ , defined by the system arriving within  $\pm 0.1$  of the eigenvalue of an eigenstate of  $S_z$ , while a  $S_z$  measurement is conducted. When the measurement strength and period are large, such as in Figure 12e, no correlations are exhibited, consistent with the Born rule. However, as the measurement strength

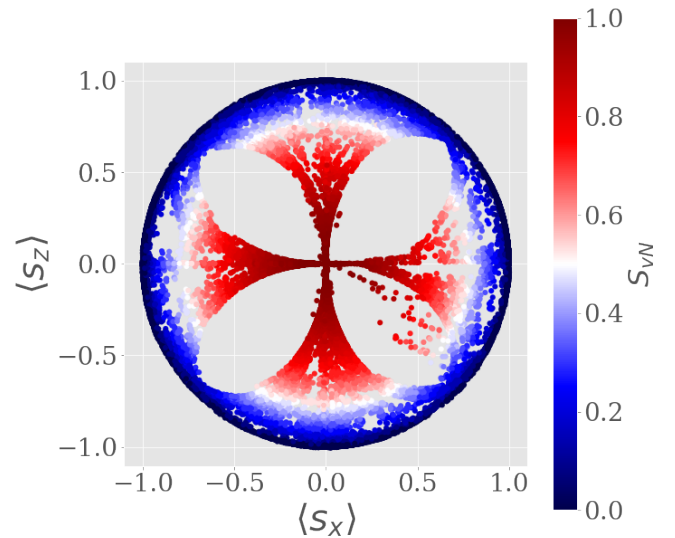


Figure 11. Color. Sample points along a trajectory in the  $(\langle S_x \rangle, \langle S_z \rangle)$  phase space of the system of entangled two-spin 1/2 subsystems indicating the degree of entanglement. The entanglement is represented by the von Neumann entropy of the reduced density matrix of one of the spin 1/2 subsystems. Measurement period 2, measurement strength 2, duration 100, time-step 0.0001. The entanglement is greatest at the centre of the circle where the maximally entangled eigenstates  $S = 1, m_x = 0$  and  $S = 1, m_z = 0$  lie and is at a minimum at the outer edge of the circle where the separable eigenstates  $S = 1, m_x = \pm 1$  and  $S = 1, m_z = \pm 1$  reside.

and period are decreased, significant correlations emerge, revealing that memory of previous outcomes of measurement of the  $S_z$  observable may be retained despite the performance of an  $S_x$  measurement in between the  $S_z$  measurements.

A second set of trajectories is now generated such that the simulation is ended when the system evolves to within  $\pm 0.1$  of certain eigenvalues of  $S_z$  and  $S_x$ , the terminating eigenstates, during the observables' respective measurement intervals. Since there are more states available to the system than for the spin 1/2 case, we can consider the probability of termination for several different combinations of terminating eigenstates. Figures 13 and 14 depict the probability of termination as a function of number of measurements performed when the terminating eigenstates are  $S = 1, m_x = -1$  and  $S = 1, m_z = -1$  and when they are  $S = 1, m_x = 0$  and  $S = 1, m_z = 0$ , respectively. Note that the first measurement corresponds to a  $S_z$  measurement, the second to a  $S_x$  measurement and the third to a  $S_z$  measurement, etc. In both Figures 13 and 14, the probability distribution resembles that generated by Born rule statistics as long as the measurement strength and period are large. Deviations from the Born rule statistics are exhibited when the measurement strength and period are lowered. Such deviations may reveal a bias towards certain eigenstates and therefore a memory of previous measurement out-

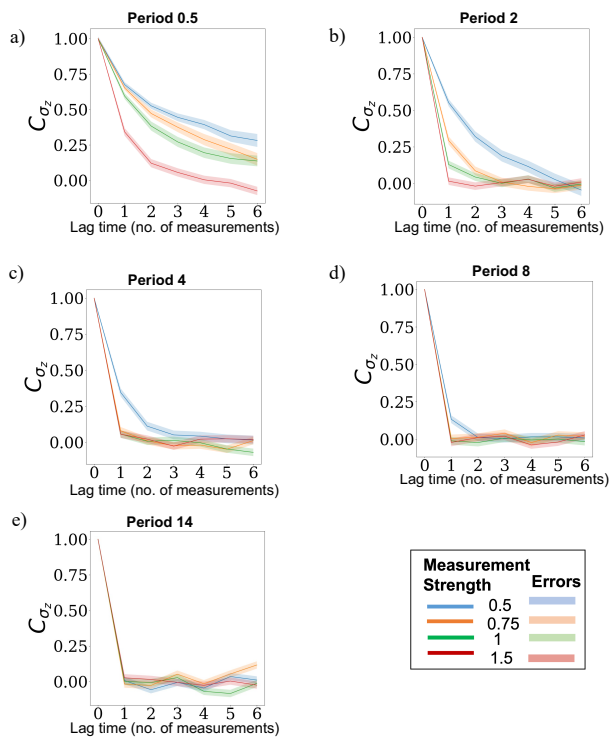


Figure 12. Color. The autocorrelation function of  $\langle S_z \rangle, C_{S_z}$ , as a function of lag time in terms of number of measurements performed, for the entangled two-spin  $1/2$  system.  $C_{S_z}$  is computed for measurement strengths 0.5, 1, 2 and 4 and for measurement periods: a) 0.5, b) 1, c) 2, d) 4 and e) 20. Duration: 1500 box function periods.

comes of the same observable. For strong, long duration measurements there is a high probability of termination after only a small number of measurements have been performed, but this probability is lower for weaker and shorter duration measurements, potentially demonstrating that the system is able to avoid certain eigenstates for longer and return to the same eigenstates as in previous measurement outcomes. There is also a higher probability of survival, after a larger number of measurements have been performed, for weaker and shorter measurements compared with stronger and longer duration ones. This effect is particularly stark in Figure 14f where the system appears to avoid the  $\langle S_z \rangle = \langle S_x \rangle = 0$  region for a large number of measurements, only collapsing at these eigenstates after at least 8 measurements have been performed. This mirrors the low probability density around these eigenstates for weaker and shorter measurements, in Figure 10a, for example.

From Figures 13 and 14 the mfp can be calculated as a function of measurement strength and period and is illustrated in Figures 15A) and B). Reflecting the trend in the probability of termination depicted in Figures 13 and 14, the mfp increases with decreasing measurement period and strength, demonstrating once again an avoidance of the terminating eigenstates for a longer time and poten-

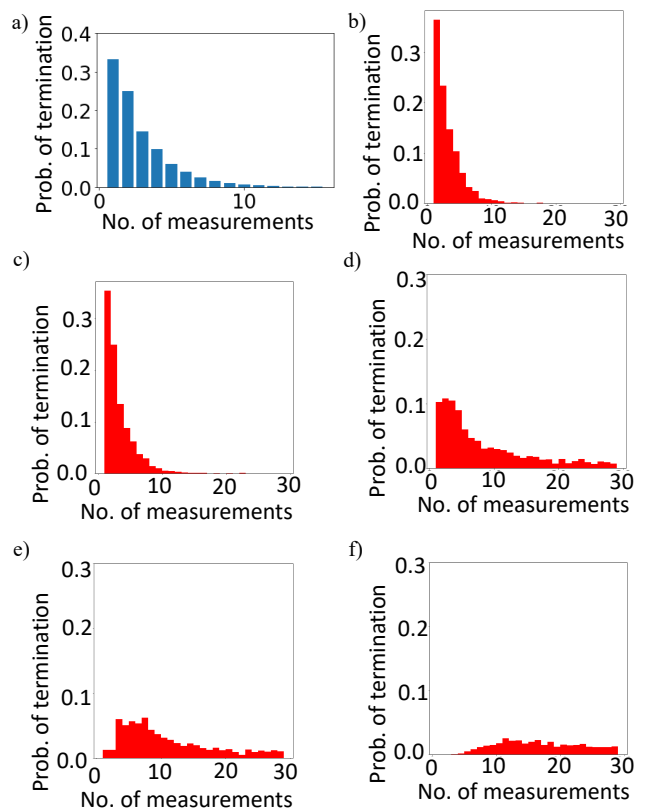


Figure 13. Probability of termination as function of number of measurements performed for the system of entangled two spin  $1/2$  subsystems. This is defined as the probability that the system will evolve to within  $\pm 0.1$  of the eigenvalues of one of the terminating eigenstates  $S = 1, m_x = -1$  and  $S = 1, m_z = -1$ , which causes the simulation to end.. Note that the first measurement corresponds to a  $S_z$  measurement, the second to a  $S_x$  measurement and the third to a  $S_z$  measurement, etc. a) Probability of termination according to the Born rule. b)-e) Numerically generated probabilities of termination obtained from 6000 trajectories, time-step 0.0001: b) Measurement period 4, measurement strength 4, c) measurement period 2, measurement strength 1, d) measurement period 1, measurement strength 1, e) measurement period 0.75, measurement strength 0.75, f) measurement period 0.5, measurement strength 0.5.

tially a bias towards return to the same eigenstates of the observables visited in previous measurements. Note that in Figure 15B), the mfp for a measurement strength of 0.5 and measurement period of 4 is exceedingly high compared to the other measurement strengths and periods, whereas the mfp for measurement strength 4, period 0.5 is considerably lower. This reveals that it is perhaps the lower measurement strength that has a greater effect on drawing the system away from the maximally entangled eigenstates of  $S_z$  and  $S_x$ , as opposed to the lower measurement period.

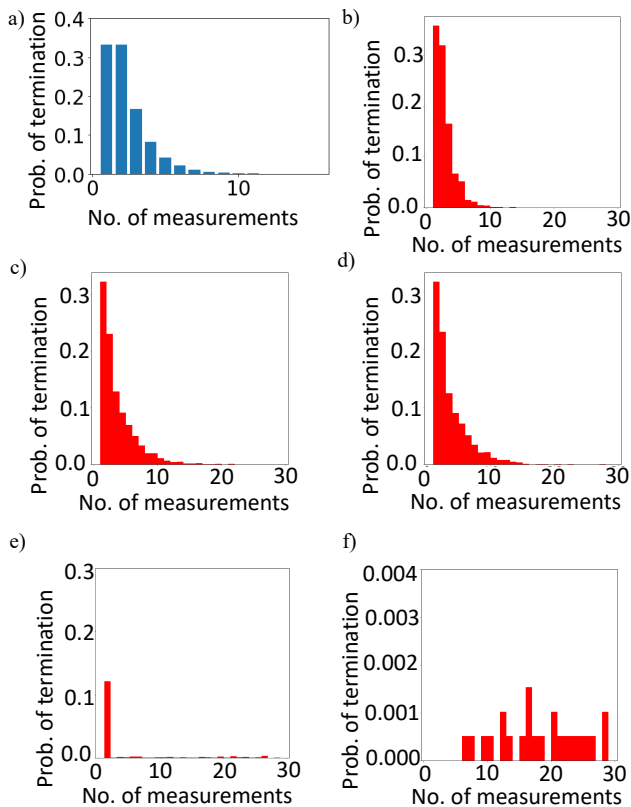


Figure 14. As Figure 13 but where  $S = 1, m_x = 0$  and  $S = 1, m_z = 0$  are the terminating eigenstates. Note that the first measurement corresponds to a  $S_z$  measurement, the second to a  $S_x$  measurement and the third to a  $S_z$  measurement, etc. a) Probability of termination according to the Born rule. b)-f) Numerically generated probabilities of termination obtained from 2000 trajectories, time-step 0.0001: b) Measurement period 4, measurement strength 4, c) measurement period 2, measurement strength 2, d) measurement period 0.5, measurement strength 4, e) measurement period 1, measurement strength 2, f) measurement period 4, measurement strength 0.5.

## VI. CONCLUSIONS

In conclusion, we have explored how memory of previous measurement outcomes of an observable in a sequence of measurements of non-commuting observables may be possible with weak and short duration measurements on a spin 1/2 system and a system of two entangled spin 1/2 subsystems. In order to generate continuous, diffusive, stochastic quantum trajectories we used the Quantum State Diffusion (QSD) formalism, which treats measurement as a dynamical interaction between a system and an environment that is designed to act as a measurement apparatus. The coupling between the system and the environment then defines the measurement strength. In order to model the sequence of measurements of observables  $S_x$  and  $S_z$ , we consider two envi-

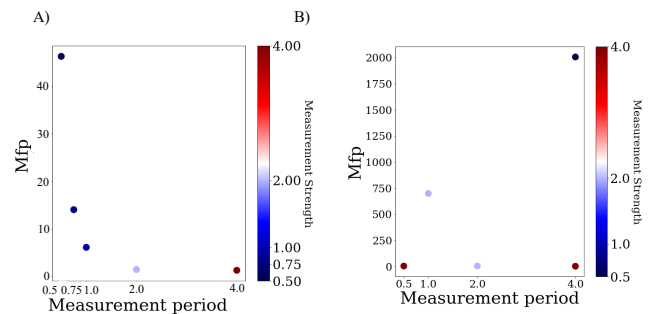


Figure 15. Color. Mean first passage (mfp) with varying measurement strength and measurement period for the system of two entangled spin 1/2 subsystems. The mean first passage is the mean number of measurements performed before the system arrives at one of the terminating eigenstates and the simulation ends. A) The mean first passage for the terminating eigenstates  $S = 1, m_x = 0$  and  $S = 1, m_z = 0$  calculated from Figure 13. The mean first passage for the terminating eigenstates  $S = 1, m_x = 0$  and  $S = 1, m_z = 0$ , calculated from Figure 14.

ronments interacting with the system, with two different measurement strengths  $a$  and  $b$  modelled as box functions in time. When  $a = 1, b = 0$  and vice-versa, such that only one measurement is performed at a time. For the spin 1/2 system we generate trajectories in the  $(r_x, r_z)$  phase space, where  $r_{x,z}$  are components of the coherence vector representing the reduced density matrix. For the entangled two-spin 1/2 system we generate trajectories in the  $(\langle S_x \rangle, \langle S_z \rangle)$  phase space.

We illustrated the trajectories for both systems using a cumulative probability density in Figures 5 and 10 which revealed that, as the measurement strength and period are lowered, the probability density in the phase space deviates from that expected of the Born rule. In particular, the probability density may be unevenly concentrated around certain eigenstates and not others. For the system of two entangled spin 1/2 subsystems, the probability density decreases starkly for the  $S = 1, m_x = 0$  and  $S = 1, m_z = 0$  eigenstates, such that the system is able to avoid them for long periods of time.

To illustrate return to particular eigenstates of the observables, demonstrating memory of previous measurement outcomes, autocorrelation functions of the  $z$ -spin component in both systems were computed and are depicted in Figures 6 and 12. The correlation between measurement outcomes were demonstrated to be significant for weak and short measurements, and to disappear for strong and long duration measurements, in accordance with the Born rule.

To further examine how long the system could avoid particular eigenstates of the observables, we introduced terminating eigenstates, defined as eigenstates of  $S_z$  and  $S_x$  which, when arrived at by the system, cause the simulation to terminate. The probability of termination, defined as the probability that the simulation ends af-

ter a certain number of measurements have been performed, was calculated, as well as the mfp, the mean number of measurements performed before the simulation terminates. We chose the  $\langle\sigma_x\rangle = -1$ ,  $\langle\sigma_z\rangle = +1$  eigenstates to be the terminating eigenstates for the spin 1/2 system, with the probability of termination depicted in Figure 7 and the mfp in Figure 8 as a function of measurement strength and period. For the system of entangled two spin 1/2 subsystems, the probability of termination and mfp for the  $S = 1, m_x = -1$  and  $S = 1, m_z = -1$  terminating eigenstates are depicted in Figures 13 and 15A). For both systems, the probability of termination closely resembles Born rule statistics for long and strong measurements, and deviates for short and weak measurements. In contrast, the strong and long measurements have a higher probability of termination after a short number of measurements compared with the shorter, weaker measurements such that the system may be able to avoid certain eigenstates of the observables. This effect is most pronounced when  $S = 1, m_x = 0$  and  $S = 1, m_z = 0$  are selected as terminating eigenstates (see Figures 14) and 15B)), such that the terminating eigenstates were avoided entirely up until at least 8 measurements had been performed for the weaker and shorter measurements, in concordance with the density plots in Figure 10. We speculate that this is because the  $S = 1, m_x = 0$  and  $S = 1, m_z = 0$  eigenstates are the only two triplet eigenstates available to the system in which the two spin 1/2 subsystems are maximally entangled. It is unclear, however, why shorter, weaker measurements should mean these eigenstates are explored less frequently and we leave this for further future exploration.

Sequences of measurements of non-commuting observables have been performed experimentally with weak measurements [5, 6, 15], and we envisage that the inves-

tigations outlined in this work could also be tested experimentally. In addition, wavefunction collapse has been experimentally observed in real-time, offering insight into the measurement timescale required to successfully complete a measurement [36, 37].

In summary, memory of previous outcomes in a sequence of measurements of non-commuting observables undergoing short and weak measurements could arise from the incompleteness of the measurement as illustrated in Figure 4. The system would not have sufficient time to collapse to an eigenstate of the second non-commuting observable and therefore it is biased towards a return to the eigenstate of the first non-commuting observable visited previously. This could operate in a similar spirit to the incomplete measurements exhibited in the partial quantum Zeno effect [38, 39] or reversed measurements, where the initial quantum state of the system is recovered after a partial measurement collapse [37, 40–42]. As such, our findings could be useful in fields of quantum state control such as in quantum computation and cybersecurity protocols, quantum state tomography, as well as quantum error correction protocols where sequences of non-commuting observables are utilised. The avoidance of the maximally entangled eigenstates of the  $S_z$  and  $S_x$  observables for the system of two entangled spin 1/2 subsystems could also be of particular interest in quantum state control.

## ACKNOWLEDGEMENTS

SMW is supported by a PhD studentship funded by EPSRC under grant codes EP/R513143/1 and EP/T517793/1.

- 
- [1] T. Norsen, *Foundations of Quantum Mechanics: An Exploration of the Physical Meaning of Quantum Theory* (Springer, Cham, Switzerland, 2017).
  - [2] M. A. Nielsen and I. Chuang, Quantum Computation and Quantum Information, *American Journal of Physics* **70**, 558 (2002).
  - [3] S. Hacoheh-Gourgy, L. S. Martin, E. Flurin, V. V. Ramasesh, K. B. Whaley, and I. Siddiqi, Quantum dynamics of simultaneously measured non-commuting observables, *Nature* **538**, 491 (2016).
  - [4] A. N. Jordan and M. Büttiker, Continuous Quantum Measurement with Independent Detector Cross Correlations, *Physical Review Letters* **95**, 220401 (2005).
  - [5] F. Piacentini, A. Avella, M. P. Levi, M. Gramegna, G. Brida, I. P. Degiovanni, E. Cohen, R. Lussana, F. Villa, A. Tosi, F. Zappa, and M. Genovese, Measuring Incompatible Observables by Exploiting Sequential Weak Values, *Physical Review Letters* **117**, 170402 (2016).
  - [6] H. F. Hofmann, Sequential measurements of non-commuting observables with quantum controlled inter-
  - actions, *New Journal of Physics* **16**, 063056 (2014).
  - [7] A. Brodutch and E. Cohen, A scheme for performing strong and weak sequential measurements of non-commuting observables, *Quantum Studies: Mathematics and Foundations* **4**, 13 (2017).
  - [8] L. A. Rozema, A. Darabi, D. H. Mahler, A. Hayat, Y. Soudagar, and A. M. Steinberg, Violation of Heisenberg’s Measurement-Disturbance Relationship by Weak Measurements, *Physical Review Letters* **109**, 100404 (2012).
  - [9] J.-S. Chen, M.-J. Hu, X.-M. Hu, B.-H. Liu, Y.-F. Huang, C.-F. Li, C.-G. Guo, and Y.-S. Zhang, Experimental realization of sequential weak measurements of non-commuting Pauli observables, *Optics Express* **27**, 6089 (2019).
  - [10] G. Mitchison, R. Jozsa, and S. Popescu, Sequential weak measurement, *Physical Review A* **76**, 062105 (2007).
  - [11] M. A. Ochoa, W. Belzig, and A. Nitzan, Simultaneous weak measurement of non-commuting observables: A generalized Arthurs-Kelly protocol, *Scientific Reports* **8**,

- 15781 (2018).
- [12] M. Ozawa, Universally valid reformulation of the Heisenberg uncertainty principle on noise and disturbance in measurement, *Physical Review A* **67**, 042105 (2003).
- [13] R. Ruskov, A. N. Korotkov, and K. Mølmer, Qubit State Monitoring by Measurement of Three Complementary Observables, *Physical Review Letters* **105**, 100506 (2010).
- [14] M. Sindelka and N. Moiseyev, Quantum uncertainties and Heisenberg-like uncertainty relations for a weak measurement scheme involving two arbitrary noncommuting observables, *Physical Review A* **97**, 012122 (2018).
- [15] Y. Suzuki, M. Inuma, and H. F. Hofmann, Observation of non-classical correlations in sequential measurements of photon polarization, *New Journal of Physics* **18**, 103045 (2016).
- [16] G. S. Thekkadath, L. Giner, Y. Chalich, M. J. Horton, J. Banker, and J. S. Lundeen, Direct Measurement of the Density Matrix of a Quantum System, *Physical Review Letters* **117**, 120401 (2016).
- [17] R. Ber, S. Marcovitch, O. Kenneth, and B. Reznik, Process tomography for systems in a thermal state, *New Journal of Physics* **15**, 013050 (2013).
- [18] Y. Kim, Y.-S. Kim, S.-Y. Lee, S.-W. Han, S. Moon, Y.-H. Kim, and Y.-W. Cho, Direct quantum process tomography via measuring sequential weak values of incompatible observables, *Nature Communications* **9**, 192 (2018).
- [19] J. S. Lundeen, B. Sutherland, A. Patel, C. Stewart, and C. Bamber, Direct measurement of the quantum wavefunction, *Nature* **474**, 188 (2011).
- [20] C. L. Clarke and I. J. Ford, Stochastic entropy production associated with quantum measurement in a framework of Markovian quantum state diffusion (2023), arxiv:2301.08197 [cond-mat, physics:quant-ph].
- [21] J. Atalaya, M. Bahrami, L. P. Pryadko, and A. N. Korotkov, Bacon-Shor code with continuous measurement of noncommuting operators, *Physical Review A* **95**, 032317 (2017).
- [22] M. Berta, M. Christandl, R. Colbeck, J. M. Renes, and R. Renner, The uncertainty principle in the presence of quantum memory, *Nature Physics* **6**, 659 (2010).
- [23] M. N. Bera, A. Acín, M. Kuś, M. W. Mitchell, and M. Lewenstein, Randomness in quantum mechanics: Philosophy, physics and technology, *Reports on Progress in Physics* **80**, 124001 (2017).
- [24] R. Prevedel, D. R. Hamel, R. Colbeck, K. Fisher, and K. J. Resch, Experimental investigation of the uncertainty principle in the presence of quantum memory and its application to witnessing entanglement, *Nature Physics* **7**, 757 (2011).
- [25] O. Calderón-Losada, T. T. Moctezuma Quistian, H. Cruz-Ramirez, S. Murgueitio Ramirez, A. B. U'Ren, A. Botero, and A. Valencia, A weak values approach for testing simultaneous Einstein–Podolsky–Rosen elements of reality for non-commuting observables, *Communications Physics* **3**, 1 (2020).
- [26] J. C. Howell, R. S. Bennink, S. J. Bentley, and R. W. Boyd, Realization of the Einstein-Podolsky-Rosen Paradox Using Momentum- and Position-Entangled Photons from Spontaneous Parametric Down Conversion, *Physical Review Letters* **92**, 210403 (2004).
- [27] A. Chantasri, J. Atalaya, S. Hacohe-Gourgy, L. S. Martin, I. Siddiqi, and A. N. Jordan, Simultaneous continuous measurement of noncommuting observables: Quantum state correlations, *Physical Review A* **97**, 012118 (2018).
- [28] J. Atalaya, S. Hacohe-Gourgy, L. S. Martin, I. Siddiqi, and A. N. Korotkov, Correlators in simultaneous measurement of non-commuting qubit observables, *npj Quantum Information* **4**, 1 (2018).
- [29] L. P. García-Pintos and J. Dressel, Probing quantumness with joint continuous measurements of noncommuting qubit observables, *Physical Review A* **94**, 062119 (2016).
- [30] Y. Suzuki, M. Inuma, and H. F. Hofmann, Violation of Leggett–Garg inequalities in quantum measurements with variable resolution and back-action, *New Journal of Physics* **14**, 103022 (2012).
- [31] Y.-F. Huang, C.-F. Li, Y.-S. Zhang, J.-W. Pan, and G.-C. Guo, Experimental Test of the Kochen-Specker Theorem with Single Photons, *Physical Review Letters* **90**, 250401 (2003).
- [32] A. Kulikov, M. Jerger, A. Potočník, A. Wallraff, and A. Fedorov, Realization of a Quantum Random Generator Certified with the Kochen-Specker Theorem, *Physical Review Letters* **119**, 240501 (2017).
- [33] C. Simon, M. Żukowski, H. Weinfurter, and A. Zeilinger, Feasible “Kochen-Specker” Experiment with Single Particles, *Physical Review Letters* **85**, 1783 (2000).
- [34] S. Hossenfelder, Testing super-deterministic hidden variables theories, *Foundations of Physics* **41**, 1521 (2011), arxiv:1105.4326.
- [35] Z. K. Mineev, S. O. Mundhada, S. Shankar, P. Reinhold, R. Gutiérrez-Jáuregui, R. J. Schoelkopf, M. Mirrahimi, H. J. Carmichael, and M. H. Devoret, To catch and reverse a quantum jump mid-flight, *Nature* **570**, 200 (2019).
- [36] A. N. Jordan, Watching the wavefunction collapse, *Nature* **502**, 177 (2013).
- [37] K. W. Murch, S. J. Weber, C. Macklin, and I. Siddiqi, Observing single quantum trajectories of a superconducting quantum bit, *Nature* **502**, 211 (2013).
- [38] A. Peres and A. Ron, Incomplete “collapse” and partial quantum Zeno effect, *Physical Review A* **42**, 5720 (1990).
- [39] M. Zhang, C. Wu, Y. Xie, W. Wu, and P. Chen, Quantum Zeno effect by incomplete measurements, *Quantum Information Processing* **18**, 97 (2019).
- [40] N. Katz, M. Neeley, M. Ansmann, R. C. Bialczak, M. Hofheinz, E. Lucero, A. O’Connell, H. Wang, A. N. Cleland, J. M. Martinis, and A. N. Korotkov, Reversal of the Weak Measurement of a Quantum State in a Superconducting Phase Qubit, *Physical Review Letters* **101**, 200401 (2008).
- [41] A. N. Korotkov and A. N. Jordan, Undoing a Weak Quantum Measurement of a Solid-State Qubit, *Physical Review Letters* **97**, 166805 (2006).
- [42] Y.-S. Kim, J.-C. Lee, O. Kwon, and Y.-H. Kim, Protecting entanglement from decoherence using weak measurement and quantum measurement reversal, *Nature Physics* **8**, 117 (2012).
- [43] W. S. Teixeira, F. L. Semião, J. Tuorila, and M. Möttönen, Assessment of weak-coupling approximations on a driven two-level system under dissipation, *New Journal of Physics* **24**, 013005 (2021).
- [44] A. Chantasri and A. N. Jordan, Stochastic path-integral formalism for continuous quantum measurement, *Physical Review A* **92**, 032125 (2015).
- [45] C. Gneiting, A. V. Rozhkov, and F. Nori, Jump-time unraveling of Markovian open quantum systems, *Physical*

- Review A **104**, 062212 (2021).
- [46] M. B. Plenio and P. L. Knight, The quantum-jump approach to dissipative dynamics in quantum optics, *Reviews of Modern Physics* **70**, 101 (1998).
- [47] G. Lindblad, On the generators of quantum dynamical semigroups, *Communications in Mathematical Physics* **48**, 119 (1976).
- [48] Y. Tanimura, Real-time and imaginary-time quantum hierarchical Fokker-Planck equations, *The Journal of Chemical Physics* **142**, 144110 (2015).
- [49] I. Percival, *Quantum State Diffusion* (Cambridge University Press, Cambridge, 1998).
- [50] N. Gisin and I. C. Percival, *Quantum State Diffusion: From Foundations to Applications* (1997), arxiv:quant-ph/9701024.
- [51] S. M. Walls, J. M. Schachter, H. Qian, and I. J. Ford, Stochastic quantum trajectories demonstrate the Quantum Zeno Effect in an open spin system (2022), arxiv:2209.10626 [cond-mat, physics:quant-ph].
- [52] M. S. Leifer, Is the quantum state real? An extended review of  $\psi$ -ontology theorems, *Quanta* **3**, 67 (2014), arxiv:1409.1570.
- [53] T. Maudlin, *Philosophy of Physics: Quantum Theory*, Princeton Foundations of Contemporary Philosophy (Princeton University Press, Princeton, 2019).
- [54] M. F. Pusey, J. Barrett, and T. Rudolph, On the reality of the quantum state, *Nature Physics* **8**, 475 (2012).
- [55] A. Petersen, The Philosophy of Niels Bohr, *Bulletin of the Atomic Scientists* **19**, 8 (1963).
- [56] N. Harrigan and R. W. Spekkens, Einstein, Incompleteness, and the Epistemic View of Quantum States, *Foundations of Physics* **40**, 125 (2010).
- [57] J. Gambetta and H. M. Wiseman, Interpretation of non-Markovian stochastic Schrödinger equations as a hidden-variable theory, *Physical Review A* **68**, 062104 (2003).
- [58] H. M. Wiseman, Quantum trajectories and quantum measurement theory, *Quantum and Semiclassical Optics: Journal of the European Optical Society Part B* **8**, 205 (1996).
- [59] S. Saunders, J. Barrett, A. Kent, and D. Wallace, *Many Worlds?: Everett, Quantum Theory, & Reality* (OUP Oxford, 2010).
- [60] D. M. Tong, J.-L. Chen, L. C. Kwek, and C. H. Oh, Kraus representation for density operator of arbitrary open qubit system, *Laser Physics* **16**, 1512 (2006), arxiv:quant-ph/0311091.
- [61] J. A. Gross, C. M. Caves, G. J. Milburn, and J. Combes, Qubit models of weak continuous measurements: Markovian conditional and open-system dynamics, *Quantum Science and Technology* **3**, 024005 (2018).
- [62] D. Matos, L. Kantorovich, and I. J. Ford, Stochastic entropy production for continuous measurements of an open quantum system (2022), arxiv:2205.07288 [cond-mat, physics:quant-ph].
- [63] C. L. Clarke, *Irreversibility Measures in a Quantum Setting*, Doctoral, UCL (University College London) (2022).
- [64] K. Jacobs, *Quantum Measurement Theory and Its Applications* (Cambridge University Press, Cambridge, 2014).
- [65] D. Aerts and M. Sassoli de Bianchi, The extended Bloch representation of quantum mechanics and the hidden-measurement solution to the measurement problem, *Annals of Physics* **351**, 975 (2014).

- [66] P. E. Kloeden and E. Platen, Stochastic Differential Equations, in *Numerical Solution of Stochastic Differential Equations*, Applications of Mathematics, edited by P. E. Kloeden and E. Platen (Springer, Berlin, Heidelberg, 1992) pp. 103–160.

### Appendix A:

The  $SU(2) \otimes SU(2)$  generators used to form the entangled two spin 1/2 system density matrix in Eq. (7) are as follows:  $\Sigma_1 = I_2 \otimes \sigma_x$ ,  $\Sigma_2 = I_2 \otimes \sigma_y$ ,  $\Sigma_3 = I_2 \otimes \sigma_z$ ,  $\Sigma_4 = \sigma_x \otimes I_2$ ,  $\Sigma_5 = \sigma_x \otimes \sigma_x$ ,  $\Sigma_6 = \sigma_x \otimes \sigma_y$ ,  $\Sigma_7 = \sigma_x \otimes \sigma_z$ ,  $\Sigma_8 = \sigma_y \otimes I_2$ ,  $\Sigma_9 = \sigma_y \otimes \sigma_x$ ,  $\Sigma_{10} = \sigma_y \otimes \sigma_y$ ,  $\Sigma_{11} = \sigma_y \otimes \sigma_z$ ,  $\Sigma_{12} = \sigma_z \otimes I_2$ ,  $\Sigma_{13} = \sigma_z \otimes \sigma_x$ ,  $\Sigma_{14} = \sigma_z \otimes \sigma_y$  and  $\Sigma_{15} = \sigma_z \otimes \sigma_z$ , where  $I_2$  is a  $2 \times 2$  identity matrix. Explicitly:

$$\begin{aligned}
 \Sigma_1 &= \begin{pmatrix} 0 & 1 & 0 & 0 \\ 1 & 0 & 0 & 0 \\ 0 & 0 & 0 & 1 \\ 0 & 0 & 1 & 0 \end{pmatrix} & \Sigma_2 &= \begin{pmatrix} 0 & -i & 0 & 0 \\ i & 0 & 0 & 0 \\ 0 & 0 & 0 & -i \\ 0 & 0 & i & 0 \end{pmatrix} \\
 \Sigma_3 &= \begin{pmatrix} 1 & 0 & 0 & 0 \\ 0 & -1 & 0 & 0 \\ 0 & 0 & 1 & 0 \\ 0 & 0 & 0 & -1 \end{pmatrix} & \Sigma_4 &= \begin{pmatrix} 0 & 0 & 1 & 0 \\ 0 & 0 & 0 & 1 \\ 1 & 0 & 0 & 0 \\ 0 & 1 & 0 & 0 \end{pmatrix} \\
 \Sigma_5 &= \begin{pmatrix} 0 & 0 & 0 & 1 \\ 0 & 0 & 1 & 0 \\ 0 & 1 & 0 & 0 \\ 1 & 0 & 0 & 0 \end{pmatrix} & \Sigma_6 &= \begin{pmatrix} 0 & 0 & 0 & -i \\ 0 & 0 & i & 0 \\ 0 & -i & 0 & 0 \\ i & 0 & 0 & 0 \end{pmatrix} \\
 \Sigma_7 &= \begin{pmatrix} 0 & 0 & 1 & 0 \\ 0 & 0 & 0 & -1 \\ 1 & 0 & 0 & 0 \\ 0 & -1 & 0 & 0 \end{pmatrix} & \Sigma_8 &= \begin{pmatrix} 0 & 0 & -i & 0 \\ 0 & 0 & 0 & -i \\ i & 0 & 0 & 0 \\ 0 & i & 0 & 0 \end{pmatrix} \\
 \Sigma_9 &= \begin{pmatrix} 0 & 0 & 0 & -i \\ 0 & 0 & -i & 0 \\ 0 & i & 0 & 0 \\ i & 0 & 0 & 0 \end{pmatrix} & \Sigma_{10} &= \begin{pmatrix} 0 & 0 & 0 & -1 \\ 0 & 0 & 1 & 0 \\ 0 & -1 & 0 & 0 \\ 1 & 0 & 0 & 0 \end{pmatrix} \\
 \Sigma_{11} &= \begin{pmatrix} 0 & 0 & -i & 0 \\ 0 & 0 & 0 & i \\ i & 0 & 0 & 0 \\ 0 & -i & 0 & 0 \end{pmatrix} & \Sigma_{12} &= \begin{pmatrix} 1 & 0 & 0 & 0 \\ 0 & 1 & 0 & 0 \\ 0 & 0 & -1 & 0 \\ 0 & 0 & 0 & -1 \end{pmatrix} \\
 \Sigma_{13} &= \begin{pmatrix} 0 & 1 & 0 & 0 \\ 1 & 0 & 0 & 0 \\ 0 & 0 & 0 & -1 \\ 0 & 0 & -1 & 0 \end{pmatrix} & \Sigma_{14} &= \begin{pmatrix} 0 & -i & 0 & 0 \\ i & 0 & 0 & 0 \\ 0 & 0 & 0 & i \\ 0 & 0 & -i & 0 \end{pmatrix} \\
 \Sigma_{15} &= \begin{pmatrix} 1 & 0 & 0 & 0 \\ 0 & -1 & 0 & 0 \\ 0 & 0 & -1 & 0 \\ 0 & 0 & 0 & 1 \end{pmatrix}.
 \end{aligned} \tag{A1}$$

### Appendix B:

Itô processes for the variables parametrising the entangled two spin 1/2 system density matrix are as follows:

$$\begin{aligned}
dv &= -\frac{1}{2}a^2vdt + a(q - v(f + p))dW_z + b(1 + h - gv - v^2)dW_x \\
de &= -\frac{1}{2}a^2edt - \frac{1}{2}b^2edt + a(s - e(f + p))dW_z + b(-e(g + v) + j)dW_x \\
df &= -\frac{1}{2}b^2fdt + a(1 - f(f + p) + u)dW_z + b(k - f(g + v))dW_x \\
dg &= \frac{1}{2}a^2gdt + a(k - g(f + p))dW_z + b(1 - g^2 + h - gv)dW_x \\
dh &= a^2(n - h)dt - ah(f + p)dW_z + b(h - 1)(g + v)dW_x \\
dj &= a^2(-j - m)dt - \frac{1}{2}b^2jdt - aj(f + p)dW_z + b(e - j(g + v))dW_x \\
dk &= -\frac{1}{2}a^2kdt - \frac{1}{2}b^2kdt + a(g - k(f + p))dW_z + b(f - k(g + v))dW_x \\
dl &= -\frac{1}{2}a^2ldt - \frac{1}{2}b^2ldt + a(o - l(f + p))dW_z + b(m - l(g + v))dW_x \\
dm &= -a^2(-j - m)dt - \frac{1}{2}b^2mdt - am(f + p)dW_z + b(l - m(g + v))dW_x \\
dn &= a^2(h - n)dt + b^2(u - n)dt - an(f + p)dW_z - bn(g + v)dW_x \\
do &= -\frac{1}{2}a^2odt + b^2(-o - s)dt + a(l - o(f + p))dW_z + bo(-g - v)dW_x \\
dp &= -\frac{1}{2}b^2pdt + a(1 - p(f + p) + u)dW_z + b(q - p(g + v))dW_x \\
dq &= -\frac{1}{2}a^2qdt - \frac{1}{2}b^2qdt - a(fq + pq - v)dW_z + b(p - gq - qv)dW_x \\
ds &= -\frac{1}{2}a^2sdt + b^2(-o - s)dt + a(e - s(f + p))dW_z + bs(-g - v)dW_x \\
du &= b^2(n - u)dt - \alpha((f + p)(-1 + u))dW_z - bu(g + v)dW_x.
\end{aligned} \tag{B1}$$


---